5th International Conference on Control Engineering&Information Technology (CEIT-2017)
Proceeding of Engineering and Technology –PET
Vol.33 pp. 40-44

Evaluation of CT to CBCT Deformable Registration Algorithms for Adaptive Radiation Therapy

KIDAR Halima Saadia[#1], AZIZI Hacene[#2], BOUKELLOUZ Wafa[*]

[#]*Department of Physics,*Department of Computer Sciences, Ferhat Abbas Setif University*
El Bez Campus 19000, Setif, Algeria

[1]kidar93@yahoo.fr, [2]azizi_hacene@yahoo.fr

Abstract— **The aim of this study is to evaluate the performance of different deformable registration (DR) algorithms. Six algorithms implemented in Elastix were used to match planning CT images to cone-beam CT (CBCT) images. The quality of the DR was evaluated using two methods; the first one consists of a visual assessment, while the second one consists of comparing the deformed CT to the CBCT images by measuring the mean squared difference (MSD) and the normalized correlation coefficient (NCC). Furthermore, the computation time for each algorithm was measured to evaluate the rapidity of registration. The results showed MSD values within 0.08 mm and NCC values close to 1 which indicates an accurate registration. In addition, compared to algorithms with adaptive stochastic gradient descent optimizer, the algorithms with gradient descent optimizers are characterized by decreased computation time, especially when combined with mutual information which increases the accuracy of registration**

Keywords— **Cone-beam CT ; Computed tomography CT; Deformable image registration; Evaluation; Adaptive radiation therapy**

I. INTRODUCTION

Recently, the integration of in-board cone beam computed tomography (CBCT) systems into linear accelerators has provided not only powerful tools for improving accuracy of patient positioning but also it makes it possible to adapt the treatment planning with patient anatomy modifications throughout the entire treatment, known as adaptive radiation therapy (ART) [1],[2]. The implementation of this technique in clinical practice goes through many complex processes such as: image registration, replanification and dose recalculation [3]. Repeated acquisition of CT images for the replanification is a time consuming procedure. Thus, it can result in high accumulated dose, which poses a health concern to patients, so that, using CBCT images is recommended [4]. However, due to their poor quality and inaccurate Hounsfield units (HUs), CBCT images cannot be directly used for ART and especially for dose calculation [5]. For that reason several studies have proposed promising techniques to correct HU values using the mapping of each HU from CT to CBCT images after rigid or deformable image registration (DIR) [6]-[8], or replacing of pixel values of CBCT by small number of fixed HU values as in CT images, which is called multilevel threshold (MLT) [8],[9]. The accuracy of these modifications is related to the choice of the registration algorithm.

By definition, image registration is the process of determining the spatial transform that maps points from one image (Fixed image) to their homologous points in another image (moving image) [10]. The registration problem is commonly considered as an optimization problem which has to be solved using an iterative way. Basically, the main framework of image registration is depicted in Fig. 1, it is composed of the following elements: (1) the input images, (2) the metrics, (3) the optimizer, (4) the sampler, (5) the transform, (6) the interpolator and (7) the pyramid. All these components are described in details in the section II-B.

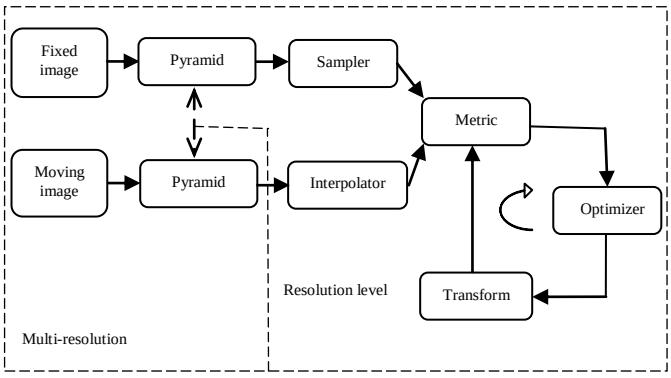

Fig. 1 The basic components of the registration framework [13]

In this study, we performed an investigation of CT to CBCT DIR using clinical data from 2 patients with prostate cancer. We evaluated the performance of several algorithms implemented in Elastix [11],[12], which are based on different components, in terms of their accuracy and calculation time.

II. METHODS AND MATERIALS

A. Image acquisition

This study was performed on datasets of 2 patients with prostate cancer, treated at the department of radiotherapy in the Cancer Center of Setif, Algeria. Each dataset contained a planning CT and CBCT images. All planning CT were obtained using GE CT scan (General Electric Medical systems) with the following settings: 100 kVp, 360 mA, 500 ms and a maximum Field of View (FoV) of 43.5 cm. These images were reconstructed on 0.8496×0.8496×3 mm grid. The CBCT images were acquired, with an on-board imager (OBI, Varian Medical Systems) mounted on the gantry of Clinical Varian iX21 linear accelerator, according to pre-defined protocols.

ISSN 2356-5608

For prostate cancer, the technical settings were: 125 kVp, 80 mA, 8567 ms, a maximum FoV of 45 cm and the images were reconstructed on 0.8789×.8789×2.5 mm grid. For all datasets CBCT images were acquired for the first day of treatment to minimize the errors of patient setup in the treatment machine.

B. Elastix

Elastix is an open source software [14] for image registration based on the Insight Segmentation and Registration Toolkit (ITK). This configurable software gives the possibility to choose several registration components to create the algorithm that suits to our needs. This part is devoted to the description of the different components used for this study.

As shown in Fig.1, the registration process passes by the definition of many elements, which are:

1) Input images: The first step in registration consists of the definition of input images which are the fixed image and the moving image.

2) Metrics: Called also similarity measures, it allows defining the quality of alignment between the two images. Several metrics can be found in Elastix, such as:

- The Mean Squared Difference (MSD), known as the simplest distance designed for mono-modal registration, it is defined as:

$$MSD(I_F, I_M) = \frac{1}{|\Omega_F|}\sum_{x_i \in \Omega_F}\left((I_F(x_i) - I_M(T(x_i))\right)^2 \quad (1)$$

  With I_F the fixed image, I_M the moving image using a given transformation T and $|\Omega_F|$ is the number of voxels of the fixed image.
- The Normalized Correlation Coefficient (NCC), it is defined as:

$$NCC(I_F, I_M) = \frac{\sum_{x_i \in \Omega_F}(I_F(x_i) - \overline{I_F})\,(T(x_i) - \overline{I_M})}{\sqrt{\sum_{x_i \in \Omega_F}(I_F(x_i) - \overline{I_F})^2\,(T(x_i) - \overline{I_M})^2}} \quad (2)$$

  With $\overline{I_F}$ and $\overline{I_M}$, the average gray values for the fixed and the moving images respectively.
- The Mutual Information (MI), which is suitable for multi-modal registration, is defined as:

$$MI(I_F, I_M) = H(I_F) + H(I_M) - H(I_F, I_M) \quad (3)$$

  Where:

$$H(I_F) = -\int p_{I_F}(a)\log p_{I_F}(a)da \quad (4)$$

$$H(I_M) = -\int p_{I_M}(b)\log p_{I_M}(b)db \quad (5)$$

  With: $H(I_F)$ and $H(I_M)$ the entropies of I_F and I_M respectively. $p_{I_F}(a)$ and $p_{I_M}(b)$ are the probabilities that has the pixels with the values a and b in I_F and I_M respectively. $H(I_F, I_M)$ is the joint entropy of I_F and I_M.
- The Normalized Mutual Information (MI), it is defined as:

$$NMI(I_F, I_M) = 1 + \frac{MI(I_F, I_M)}{H(I_F, I_M)} = \frac{H(I_F) + H(I_M)}{H(I_F, I_M)} \quad (6)$$

3) Image samplers: The samplers define the way to select a subset of voxels for the metric calculation. The most common samplers in Elastix are:

- The Random Sampler, it selects a number of voxels from I_F, whose coordinates form x_i. Every voxel has equal chance to be selected.
- The Random Coordinate, it is similar to a Random Sampler, but this one is not limited to voxel positions. Coordinates between voxels can also be selected.

4) Interpolators: An interpolator is used to evaluate the intensities in the moving image at non-voxel positions. For this work we used:

- The N^{th} Order B-Spline Interpolator, for this interpolator the higher the order the better the quality.

5) Transforms: The transform is defined as mapping from the fixed image to the moving image. Several types of transformations are included in Elastix, we cite:

- The Rigid transformation, it allows to treat the image as a rigid body, which can translate and rotate. It can be described by the following formula:

$$T(x) = R(x - c) + t + c \quad (7)$$

  With R a rotation matrix, c the center of rotation and t the translation.
- The Affine transformation, it gives more degrees of freedom to the image, which means that the image can be translated, rotated, scaled and sheared. It is defined as:

$$T(x) = A(x - c) + t + c \quad (8)$$

  Where A matrix without restrictions.
- The B-splines transformation, it is defined as non-rigid or deformable transformation. It can be described as follows:

$$T(x) = x + \sum_{x_k \in N_x} p_k \beta^3\left(\frac{x - x_k}{\sigma}\right) \quad (9)$$

  With x_k the control points, $\beta^3(x)$ the cubic multidimensional B-spline control points spacing and N_x the set of all control points within the compact support of the B-spline at x.

6) Optimizers: This element aims to find the optimal metric value giving the most accurate alignment. For this study we used two types of optimizers, which are:

- The Gradient Descent (GD), it takes the search direction as the negative gradient of the cost function, it is defined as:

$$\mu_{k+1} = \mu_k + a_k g(\mu_k) \quad (10)$$

  With $g(\mu_k) = \partial C/\partial \mu$, the gradient at the position μ_k and $a_k = a/(k + A)^{\alpha}$ the decaying function where $a > 0$, $A \geq 1$ and $0 \leq \alpha \leq 1$ are user defined constants.
- The Adaptive Stochastic Gradient Descent (ASGD), it is an advanced version of GD which requires less parameters to be set and tends to be more robust [15].

7) *Pyramids:* The use of pyramid allows starting the registration from images with low complexity (smoothed or down-sampled) to images with high complexity. For this study we used one type of pyramids which is:

- The Gaussian scale space, it applies smoothing and no down-sampling.

Table 1 recapitulates the different component with their names as indicated in Elastix and the different parameters used. For all the algorithms we used the same interpolator, sampler and pyramids but different metrics and optimizers were used.

C. Image pre-processing

Initially, the deformable registration was performed using images in which the couches of the CT scanner and the linear accelerator were present. So, to evaluate the impact of couch on the quality of registration, FIJI software [16] was used to select the region which contains only the body contour and remove the couches from images. Then, the results of registration for the images with and without couches were compared.

D. Images Alignment

Before starting the DR, the datasets for each patient were rigidly registered, using the rigid transformation described in the section II-B-5, in order to ensure a good alignment between images and improve the speed of the DR.

E. Evaluation

The accuracy of the registration was evaluated by two different methods. The first one consisted of using VV image viewer [17] to perform a visual assessment. This software allows comparing the deformed moving images (planning CT in our study) to the fixed images (CBCT) by superimposing them using complementary colors. The second method consisted of a quantitative evaluation; it was mainly based on the measures of similarity between the deformed moving images and the fixed images using Elastix. For this comparison we used as metrics, the MSD and the NCC described in the section II-B-2.

F. Computation time

The consumed time to perform the registration is an important criterion to accept or refuse the algorithm for the clinical practice, therefore, the computation time for each algorithm were measured. For this study, all the calculations were done on Intel® Core™ i5-3230M CPU (2.60 GHz, 4 GB RAM).

III. Results and Discussion

A. Qualitative evaluation

Fig. 2(a) and (b) shows respectively the CBCT and CT slices used for this study. Generally, the number of slices acquired for these two types of tomography is not the same. Therefore, the superimposition of all slices can lead to a miss-alignment between the CBCT and CT images as shown in Fig. 2(c). To deal with this problem a RR was applied resulting in a good global alignment (Fig. 2(d)), whereas in specific regions as the bony regions a poor registration can be observed.

Fig. 3 presents the results of superimposition of the CBCT images (fixed images) and the deformed CT images by applying different DR algorithms. As shown in Figs. 3(a), (b) and (c), the use of the GD with MI, NCC and NMI results in good alignment between anatomical structures but with some differences in body contours due to the fact that the algorithms based on GD depends on the increased amount of scatter present in CBCT images. On the other hand, the Figs. 3 (c), (d) and (e), in which a combination of ASGD with MI, NCC and NMI were used, show an excellent alignment between anatomical structures and also body contours which demonstrate the independency of those algorithms on the quality of CBCT images.

TABLE I
SUMMARY OF STUDY ALGORITHMS WITH THEIR DIFFERENT COMPONENTS AND PARAMETERS

Algorithm number	**Components**								
	Transform	**Metric**	**Optimizer**		**Interpolator**		**Sampler**		**Pyramids**
	Name	**Name**	**Name**	**Parameter**	**Name**	**Parameter**	**Name**	**Parameter**	**Name**
1	Deformable Registration (BSpline Transform)	AdvancedMattes MutualInformation	Standard Gradient Descent	A = 50 a = 2000 α = 0.602	BSpline Interpolator	Number of iterations = 300	Random Coordinate	Number of Samples= 3000	Fixed Smoothing Image Pyramid & Moving Smoothing Image Pyramid
2		AdvancedNormalized Correlation				Number of iterations = 500			
3		NormalizedMutual Information							
4		AdvancedMattes MutualInformation	Adaptive Stochastic Gradient Descent	Automatic determination of A, a and α		Number of iterations = 300			
5		AdvancedNormal ized Correlation				Number of iterations = 500			
6		NormalizedMutual Information							

α and a : constants defined by the user, A: 10% of the maximum number of iterations.

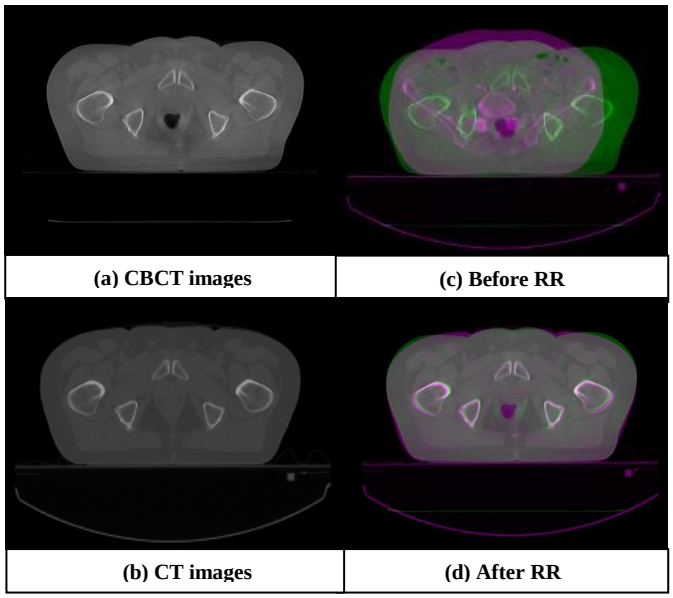

Fig. 2 A slice of cone-beam CT (a) and the planning CT (b) and the results of superimposition of CT & CBCT before alignment (c) and after alignment (d) with rigid registration

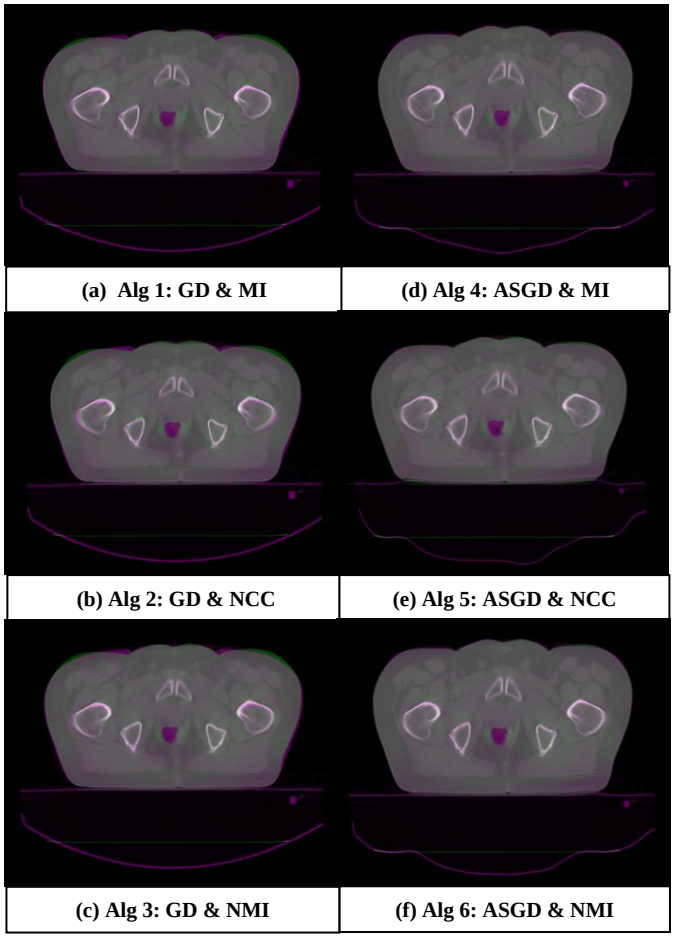

Fig. 3 The results of superimposition of CBCT images and deformed CT images by applying six DR algorithms based on (a) GD and MI (b) GD and NCC (c) GD and NMI (d) ASGD and MI (e) ASGD and NCC (f) ASGD and NMI.

B. Quantitative evaluation

Fig. 4 illustrates the results of comparison of CBCT and deformed CT images with and without couches using the MSD for which the lower the metric value, the better the registration. For the two patients, we observe acceptable values of MSD ranging from 0.115 to 0.128 mm for the algorithms based on GD, while we achieve a better registration accuracy for the algorithms based on ASGD optimizer with lower MSD values ranging from 0.055 to 0.067 mm. Thus, the pre-processing of CBCT and CT images by removing the couches before applying the DR decreased the MSD values from about 0.12 mm to lower values of about 0.06 mm. Besides, regarding the combination of GD or ASGD with MI, NCC or NMI, the results show that in the most of cases the use of GD with MI and ASGD with NCC can improve the quality of registration giving decreased values of MSD compared to the other algorithms.

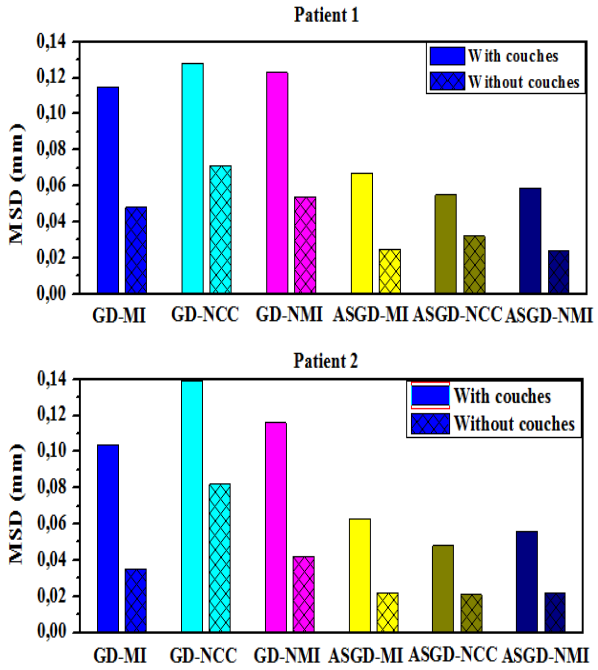

Fig. 4 Comparison of the MSD between CBCT and deformed CT images with and without couches for the two patients using the different algorithms.

In the same way, Fig. 5 presents the results of comparison of CBCT and deformed CT images with and without couches using the NCC for which the optimum is reached for metric value of -1. The measured values of NCC are presented in absolute values as visible in Fig. 5. For the two patients, the results show a good correlation between CBCT and deformed CT with NCC values close to 1. In addition, the DR based on images without couches yielded more accurate results of about 0.99 which confirm the advantages of the pre-processing of CT and CBCT images. Furthermore, the use of GD with MI and ASGD with NCC for an accurate DR is confirmed. Thus, we can say that applying these two algorithms on pre-processed CT and CBCT images allows the gain in terms of accuracy.

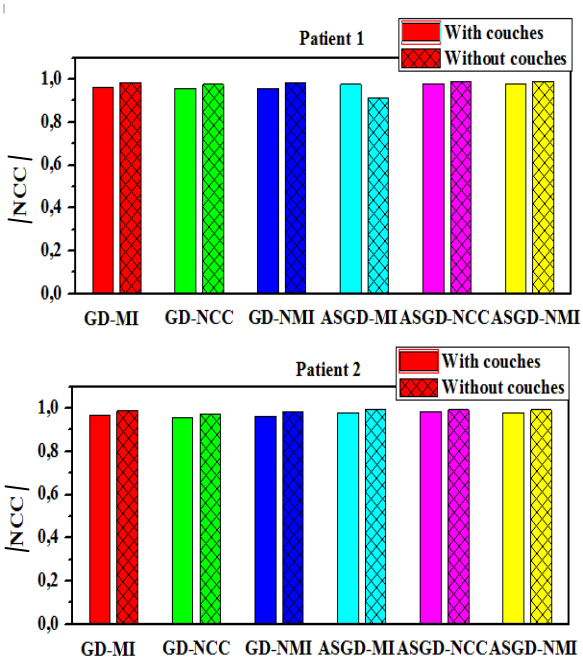

Fig. 5 Comparison of the NCC between CBCT and deformed CT images with and without couches for the two patients using the different algorithms.

The results of the required time to complete the registration are summarized in Table II. When comparing the obtained results for each algorithm a large variability can be observed. We found that the DR with ASGD is two times longer than using the GD optimizer. Also, the use of ASGD or GD with NMI and NCC remained in most cases a time consuming process while the combination of GD with MI ran in a shorter time. Moreover, the computation time is markedly reduced when using pre-processed images. So, referring to all these results, the use of GD-MI with modified CT and CBCT images enables us to gain in terms of rapidity.

TABLE II
COMPARISON OF THE COMPUTATION TIME FOR EACH ALGORITHM USING IMAGES WITH AND WITHOUT COUCHES

Algorithm	**Patient 1**		**Patient 2**	
	With couches	**Without couches**	**With couches**	**Without couches**
GD-MI	16 min 3.9 s	10 min 7.5 s	9 min 59.2 s	10 min 39.6 s
GD-NCC	16 min 11 s	11 min 43.7 s	10 min 6.3 s	10 min 15.2 s
GD-NMI	32 min 55.8 s	18 min 49.9 s	19 min 21.5 s	19 min 8 s
ASGD-MI	29 min 50.6 s	17 min 45.9 s	31 min 57.4 s	19 min 59.7 s
ASGD-NCC	29 min 58.8 s	16 min 8.6 s	28 min 46.3 s	18 min 10.3 s
ASGD-NMI	50 min 42.1 s	33 min 31.1 s	44 min 18.2 s	27 min 16.1 s

IV. CONCLUSION

We evaluated the accuracy of DR algorithms for CBCT and CT images of two patients with prostate cancer. The results showed that MSD values were within 0.08mm and NCC values were close to 1for pre-processed images and which were better than DR using CBCT and CT images without any modification. Moreover, considering that using GD-MI or ASGD-NCC leads to an accurate registration but with a significant difference in computation time, working with GD-MI seems more appropriate to benefit on accuracy and rapidity. On the basis of this study, the implementation of these algorithms on GPU card is proposed to decrease the required time to complete the registration making it possible to implement online-ART in clinical practice after the enhancement of the quality of CBCT images.

REFERENCES

[1] A. Vestergaars, L. Muren, J. Sondergaard, U.V. Elstrom et al, "Adaptive plan selection vs. Re-optimisation in radiotherapy for bladder cancer: a dose accumulation comparison," Radiother. Oncol, vol.109, pp. 457-462, 2013.

[2] F. Pos, M. Hulshof, J. Labesque et al, "Adaptive radiotherapy for invasive bladder cancer: a feasibility study," Int. J. Radiot. Oncol. Biol. Phys, vol. 64, pp. 862-868, 2006.

[3] C.Lafond, A.Simon, O.Henry, N.Prichon, "Radiothérapie adaptative en routine? Etat de l'art: point de vue du physicien médical, " Cancer. Radiothérapie, (2015).

[4] G. X. Ding, D. M. Duggan, C. W. Coffey, M. Deeley at al, "A study on adaptive IMRT treatment planning using kv cone-beam CT," Radiother. Oncol, vol. 85, pp. 116-125, 2007.

[5] A. Richter, Q. Hu, D. Steglich, K. Baier, J. Wilbert, M, Guckenberger et al, "Investigation of the usability of conebeam CT data sets for dose calculation," Radiat. Oncol, vol. 3, no. 42, December 2008.

[6] Y. Yang, E. Schreibmann, T. Li, C. Wang, L. Xing, "Evaluation of on-board kv Cone beam CT (CBCT)-based dose calculation," Phys. Med. Biol, vol. 52, pp. 685-705, 2007.

[7] M. Chao, Y. Xie, L. Xing, "Auto-propagation of contours for adaptive prostate radiation therapy," Phy. Med. Biol, vol. 53, pp. 4533-4542, 2008.

[8] Y. Onozato, N. Kadoy, Y. Fujita, K. Arai, S.Dobashi, K.Tekeda, et al, "Evaluationof on board kv cone-beam computed tomography-based dose calculation with deformable image registration using hounsfeild unit modification," Int. J. Radiot. Oncol. Biol. Phy, vol. 89, pp. 416-23, 2014.

[9] T. Almatani, R. P. Hugtenburg, R. D. Lewis, S. E. Barley, M. A. Edwards, Automated algorithm for CBCT- based dose calculations of prostate radiotherpay with bilateral hip protheses," Br. J. Radiol, vol. 89, no. 20160443, 2016.

[10] C. Boydev, "Automatic segmentation of cone-beam computed tomography images for prostate cancer radiation therapy," Doc. thesis, University of Valenciennes and Hainaut-Cambresis, France, 2015.

[11] S. Klein, M. Staring, K. Murphy, M. A. Viergever, J. P. W. Pluim, "Elastix: a toolbox for intensity based medical image registration," IEEE transactions on medical imaging, vol. 29, no. 1, pp. 196-205, Jan. 2010.

[12] D. P. Shamonin, E. E. Bron, B. P. F. Lelieveldt, M. Smits, S. Klein, M. Staring, "Fast parallel image registration on CPU and GPU for diagnostic classification of Alzheimer disease," Frontiers in Neuroinformatics, vol. 7, no. 50, pp. 1-15, Jan. 2014.

[13] S. Klein, M. Staring, Elastix manual, Sep.2015.

[14] (2004) The ELASTIX website. [Online]. Available: http://elastix.isi.uu.nl/index.php

[15] S. Klein, J. P. W. Pluim, M. Staring, M. A. Viergeiver, "Adaptive stochastic gradient descent optimization for image registration," Int. J. Comp. Vis, Vol. 81, no. 3, pp. 227-239, March 2009.

[16] (2007) The FIJI website. [Online]. Available: https://imagej.net/Fiji

[17] (2011) The VV website. [Online]. Available: https://www.creatis.insa-lyon.fr/rio/vv/